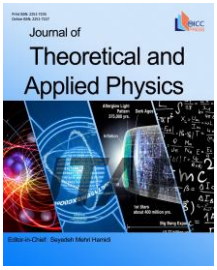

J. Theor. Appl. Phys., 2026; 20(2): 185-195

Journal of Theoretical and Applied Physics (JTAP)

https://doi.org/10.57647/jtap.2026.2002.12

Research Article

Optimization of Copper Ion Concentration into the Lattice of Barium Sulphide Nanoparticles Synthesized via a Chemical Approach

McDonald Chukwudi Okafor[1], Lawrence Ese Esiekpe[1], Vivian Anulichukwu Attoh[1], Nwando Blessing Okeke[1], Azuka Bright Okwuelum[1], Joseph Onyeka Emegha*[2]

[1]*Department of Physics Education, Federal College of Education (Technical) Asaba, Delta State, Nigeria*
[2]*Department of Physics, Hensard University, P.O.Box 1036, Yenagoa, Bayelsa State, Nigeria*

***Corresponding author:** jjjemegha@yahoo.com

Article History:

Received:
23 August 2025

Revised:
26 October 2025

Accepted:
25 December 2025

Published Online:
05 February 2026

Published in Issue:
30 April 2026

Abstract

Copper barium sulphide ($Cu_xBa_{1-x}S$) thin films (TFs) were fabricated via the chemical bath deposition (CBD) approach on glass substrates. The study used solutions of copper (II) sulphate, barium chloride dihydrate, and thiourea as the sources of the elements (copper, barium, and Sulphur). The thin films were characterized using the x-ray diffraction (XRD), scanning electron microscopy (SEM), energy-dispersive X-ray (EDX) and ultraviolet-visible spectroscopy. XRD examination of the films revealed that they were polycrystalline and increased with doping concentrations. However, increasing copper incorporation led to an increase in the average crystallite sizes from 18.80 to 21.96 nm, accompanied by a decrease in dislocation density (δ) (2.83×10^{-3} to $2.08 \times 10^{-3} nm^{-3}$), and strain (ε) ($1.84 \times 10^{-3}$ to 1.58×10^{-3}) respectively. Energy-dispersive X-ray analysis reveals good agreement between detected and selected element ratios with different stoichiometry. Optical examination indicated that $Cu_xBa_{1-x}S$ TFs have a transmittance that increased from 20% to 50% with an increase in copper concentrations, while the optical band gap varied from 1.65 to 3.12 eV. These results indicate that the synthesized $Cu_xBa_{1-x}S$ TFs hold significant potential for applications in solar energy and optoelectronics.

Keywords: Barium Sulphide, Optical Characterization, Chemical Bath Deposition, Thin Films, Copper Concentration

Cite this article: Okafor, M. C.,.Esiekpe, L. E., Attoh, V. A., Okeke, N. B., Okwuelum, A. B. & Emegha, J. O., (2026) Optimization of Copper Ion Concentration into the Lattice of Barium Sulphide Nanoparticles Synthesized via a Chemical Approach. J. Theor. Appl. Phys., 20(2), 185-195. https://doi.org/10.57647/jtap.2026.2002.12

1. Introduction

The widespread pollution caused by traditional energy sources necessitates a strong shift towards renewable and sustainable alternatives [1, 2]. Solar energy is a highly efficient and renewable alternative that researchers have extensively developed to convert sunlight photons into useful electrical energy for numerous applications [1- 4]. The application of thin films (TFs) in solar cell fabrication is currently of great interest to researchers and industrialists

because of their excellent properties, such as a tunable band-gap, low production cost, and ease of forming charge pairs, which enables the conversion of photons to electricity [5, 6]. Although thin-film solar cell-based photovoltaic modules like CdTe and Cu(In,Ga)Se_2 have demonstrated remarkable efficiencies of over 20% [7], their toxicity has been a significant concern [7, 8]. However, to be a practical source of green energy for the society, thin film solar panels must be manufactured on a wide scale using inexpensive, readily available, and environmentally benign components [9].

Copper zinc sulphide (CZS), copper zinc tin sulphide (CZTS), and copper aluminum oxide ($CuAlO_2$) are among the recently created, inexpensive, and nontoxic copper-based-nanoparticle compounds that have shown the highest efficiency in solar cell fabrication [9, 10]. Nevertheless, these materials still have a lot of issues [10]. For example, their limited single phase region in the phase diagram and their numerous secondary phases within the material prevent future advancements in cell efficiency [5, 9 - 11]. Current research efforts are increasingly directed towards copper barium sulphide ($Cu_xBa_{1-x}S$) thin films, a ternary semiconductor compound valued for its abundance in the earth's crust and low toxicity [9]. This I-II-VI semiconductor material is characterized by a desirable band gap, significant transparency, and a high absorption coefficient (around $10^5 cm^{-1}$), attracting considerable interest from researchers working on optical detectors, light-emitting diodes, solar cells, and nonlinear optics [7 – 9]. Also, it exhibits a stable structure at room temperature, making the thin film well-suited for photo-electronic applications due to their proximity to the optimal region of the visible solar energy spectrum [7, 11 - 13].

Various methods have been employed for the deposition of copper-based-nanoparticle TFs, including solution-base spin coating synthesis [11, 14], sputtering [12], RF magnetron co-sputtering [13], and hydrothermal method [15 – 17]. Although these procedures produce crystalline or amorphous films, their cost, ease of large-scale production, and temperature make them undesirable [18]. The chemical bath deposition (CBD) technique is recognized as one of the most straightforward and cost-effective methods due to its requirement of very low synthesis temperatures, good uniformity, reproducibility, suitability for various substrates, and capability for large-scale production [19 - 21]. Consequently, the application of the CBD technique has garnered significant attention due to its great potential for fabricating high-quality films [21]. Historically, CBD was used to synthesize crystalline and polycrystalline binary sulphides and oxides. More recently, the CBD technique has been sought after for synthesizing high quality ternary thin films materials for device applications [5].

Review of literature showed that the microstructural parameters and optical properties of polycrystalline $Cu_xBa_{1-x}S$ thin films is scarce. Moreover, detailed compositional analysis in many ternary nano-materials studies is limited by preparation challenges. Consequently, this study's primary objective was to synthesize ternary $Cu_xBa_{1-x}S$ thin films using the CBD method, chosen for its distinct advantages in substrate deposition [5, 21]. Secondly, the authors investigate how varying copper content impacts the films' compositional structure, thereby enhancing their optical and opto-electrical performance. Therefore, this work aims to investigate the crystallographic, microstructural, and optical properties of $Cu_xBa_{1-x}S$ thin films, including their dependence on film composition and Cu-ratios. The material was chosen because it has good optical and electrical properties and are less toxic when compare to other ternary materials like copper zinc telluride ($CuZnTe_2$), copper zinc selenide ($CuZnSe_2$) and copper aluminium selenide ($CuAlSe_2$). Besides, the authors specifically studied the microstructural properties of $Cu_xBa_{1-x}S$ thin films and related them to optical transmittance, bandgap, refractive index, extinction coefficient, and dielectric constants for device applications.

2. Materials and method

2.1. Chemicals

Copper barium sulphide TFs were prepared using pure chemicals of analytical grade, employed exactly as purchased.

The chemicals included copper (II) sulphate ($CuSO_4$) [Assay, % purity = 99.0], ammonia solution (NH_4OH) [AlfaChem India, % purity = 99.3], barium chloride dihydrate ($BaCl_2.2H_2O$) [Akshya Chemicals Pvt. % purity = 99.0%], thiourea ($CS(NH_2)_2$ [LABOSI, % purity = 98.0], triethanolamine [TEA] ($C_6H_{15}NO_3$) [Stenfy Chemicals, % purity = 99.0], ethylenediaminetetraacetic acid (EDTA) [ArochemPvt. % purity = 98.0%], and distilled water.

2.2. Preparation of copper barium sulphide TFs

The procedure for cleaning the substrate and creating the precursor is based on one of our recent works [22]. A two-step chemical precursors techniques was employed to synthesized $Cu_xBa_{1-x}S$ thin films onto glass substrates. In solution I, for copper sulphide (CuS) preparation, 0.2 M copper (II) sulphate was dissolved with 0.5 M thiourea and three drops of triethanolamine in a 50 mL beaker. In solution II, for barium sulphide (BaS) preparation, 0.3 M barium chloride dihydrate was dissolved in 0.5 M thiourea

with four to five drops of ethylenediaminetetraacetic acid in a different 50 mL beaker. However, the $Cu_xBa_{1-x}S$ thin films were obtained by mixing precursors solutions of CuS and BaS based on the ratios detailed in Table 1. These mixtures were thoroughly stirred and deposited using the setup illustrated in Figure 1, then left at room temperature for 12 hours. This procedure yielded three thin-film samples of copper barium sulphide ($Cu_xBa_{1-x}S$), labeled A1 or $Cu_{10}Ba_{90}S$, A2 or $Cu_{30}Ba_{70}S$, and A3 or $Cu_{50}Ba_{50}S$, each possessing a different concentration of the material.

Table 1. Percentage combination of $Cu_xBa_{1-x}S$ TFs

Samples	Precursors Ratio	Thickness
$Cu_{10}Ba_{90}S$	10% Copper Sulphide + 90% Barium Sulphide	68.60
$Cu_{30}Ba_{70}S$	30% Copper Sulphide + 70% Barium Sulphide	74.42
$Cu_{50}Ba_{50}S$	50% Copper Sulphide + 50% Barium Sulphide	80.16

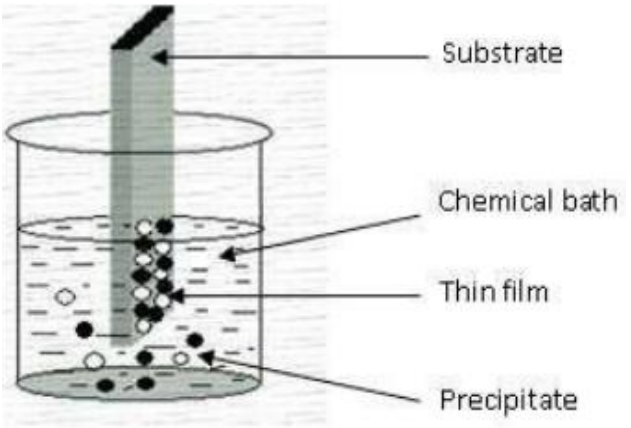

Figure 1. Chemical bath deposition setup [23]

2.3. Characterization of the deposited TFs

The crystallinity of $Cu_xBa_{1-x}S$ TFs was examined via a D8-High Resolution x-ray diffractometer (XRD) with λ = 1.5406 Å.

Scanning electron microscope (SEM) machine, model JEOL JSM-7600F incorporated with Electron dispersive x-ray (EDX) analyser was employed to study the morphological structures of the deposited films at 1000 V. For optical characterization, a Double Beam UV-1800s Shimadzu Spectrophotometer was used to measure wavelengths ranging from 300 to 1100 nm. The thickness of the film was measured using the weight difference method using the relations: $t = \frac{M}{2AD}$, and $M = m_a - m_b$. Here m_a is the mass of the substrates before deposition, and m_b is the mass of the substrates after deposition. A is the area of the deposited surface and D is the density of the material.

3. Results and discussion

Figure 2 illustrations the XRD patterns of the deposited $Cu_xBa_{1-x}S$ TFs. The results indicate that the film is polycrystalline, with five major peaks at 12.08°, 17.06°, 26.89°, 40.0°, and 56.24° corresponding to the diffraction lines of (112), (121), (111), (211), and (311), representing an orthorhombic α-phase crystalline structure (# PDF 98-001-9167) [24]. The Figure shows peak patterns in the samples that was increasing as copper concentrations rise. The peaks of Samples $Cu_{10}Ba_{90}S$ were seen to increase gradually with rise in copper concentrations. This indicates a progressive transformation from the barium-sulphide-binary phase to a distinct, oriented, polycrystalline $Cu_xBa_{1-x}S$ structure, suggesting a unification of the binary components into the deposited ternary $Cu_xBa_{1-x}S$ thin films as the copper concentration increases [25]. The polycrystalline structure of the deposited material in Samples $Cu_{30}Ba_{70}S$ and $Cu_{50}Ba_{50}$ shows varying peak orientation as they shift to the (101) plane. This phenomenon may be attributed to a chemical reaction between the film's precursors, leading to the formation of a new chemical phase [5, 21]. The observed variations in the deposited ternary films suggest that the elements within the ternary system can integrate and substitute within the matrix without significant distortions as doping levels increase [26]. Comparable outcomes have been reported in the literature by Ref. [27], and were attributed to the nature of the substrates used as well as the presence of other phases not observed by the XRD measurement.

Moreover, the impact of copper incorporation on the crystallite size (D_x), dislocation density (δ), and strain (ε) of the nanostructured $Cu_xBa_{1-x}S$ thin film were investigated on (101) plane by employing the Debye–Scherrer formula [28, 29].

$$D_x = \frac{0.9\,x\,\lambda}{\beta\cos\theta} \quad (1)$$

$$\delta = \frac{1}{D^2} \quad (2)$$

$$\varepsilon = \frac{\beta\cos\theta}{4} \quad (3)$$

In these formulas, the diffraction angle is denoted by θ, the full width at half maximum (FWHM) of the diffraction angles is given by β, and λ is the X-ray wavelength (λ = 1.54). Table 2 depicts the estimated XRD parameters for $Cu_xBa_{1-x}S$ thin films. The table shows that as the copper concentration increases, both dislocation density (δ), and strain (ε) decrease, while the crystallite size (D_x) increases from 18.80 to 21.95 nm. The development in the crystallite size could be ascribed to the incorporation of copper ions

into the barium sulphide lattice, where they substitute for Ba^{2+} ions. This substitution introduces strains and defects within the barium sulphide lattice, disrupting the regular crystal structure and promoting the formation of larger crystallites.

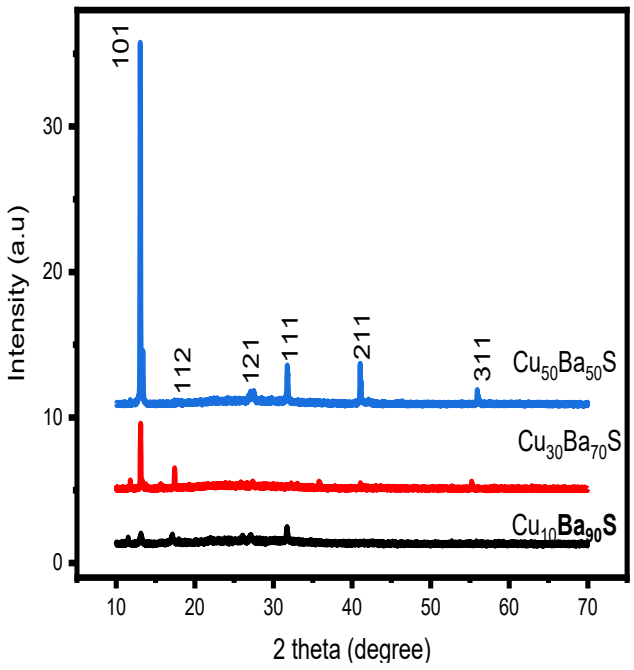

Figure 2. XRD pattern of $Cu_xBa_{1-x}S$ TFs

Table 2. XRD parameter of $Cu_xBa_{1-x}S$ TFs

Samples	D_x (nm)	δ x 10^{-3} (nm^{-3})	ε x 10^{-3}
$Cu_{10}Ba_{90}S$	18.80	2.83	1.84
$Cu_{30}Ba_{70}S$	19.28	2.69	1.79
$Cu_{50}Ba_{50}S$	21.95	2.08	1.58

Table 3. Elemental parameters of $Cu_xBa_{1-x}S$ TFs

Samples	Elemental Composition (%)			(Cu + Ba)/S
	Cu	Ba	S	
$Cu_{10}Ba_{90}S$	32.09	25.81	41.10	1.41
$Cu_{30}Ba_{70}S$	30.53	28.33	40.92	1.44
$Cu_{50}Ba_{50}S$	29.40	30.70	30.20	1.53

Additionally, the presence of copper induces compressive stress and lattice distortion, further influencing the growth of crystallites [6, 30]. Figure 3 illustrates the surface morphologies of $Cu_xBa_{1-x}S$ thin films at various concentration. The surface morphology clearly indicates that the copper concentration impacts the phases displayed by the films. Samples $Cu_{10}Ba_{90}S$ and $Cu_{30}Ba_{70}S$ feature partially dense, well-defined columnar nano-grains on some areas of the substrates (Figure 3(a, b)). As the copper concentration increases, the nano-grains increase in size, forming clusters that develop into larger grains with well-defined grain boundaries, as shown in Figure 3(c) for sample $Cu_{50}Ba_{50}$. This enhanced morphology is consistent with XRD results, which show that higher copper contents produce more uniformly sized grains, characteristic of well-ordered crystal structures [26].

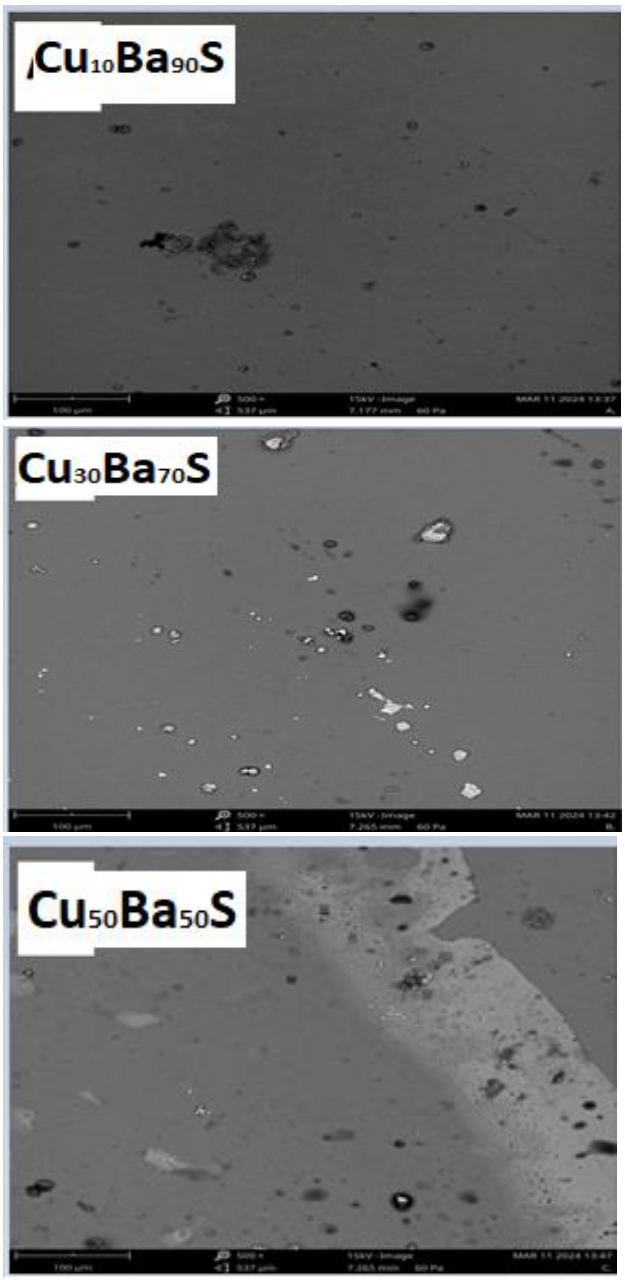

Figure 3. SEM pattern of $Cu_xBa_{1-x}S$ TFs

The main reason is that a higher copper concentration leads to fewer defects in the material's structure and also enhances its crystalline roughness [5, 21].

This rough texture is beneficial for photovoltaic manufacturing as it helps to capture more photons, which in turn boosts the absorption and current densities within the thin films [5]. Furthermore, the absence of cracks in all deposited films is a crucial factor for their use in sensing applications [31].

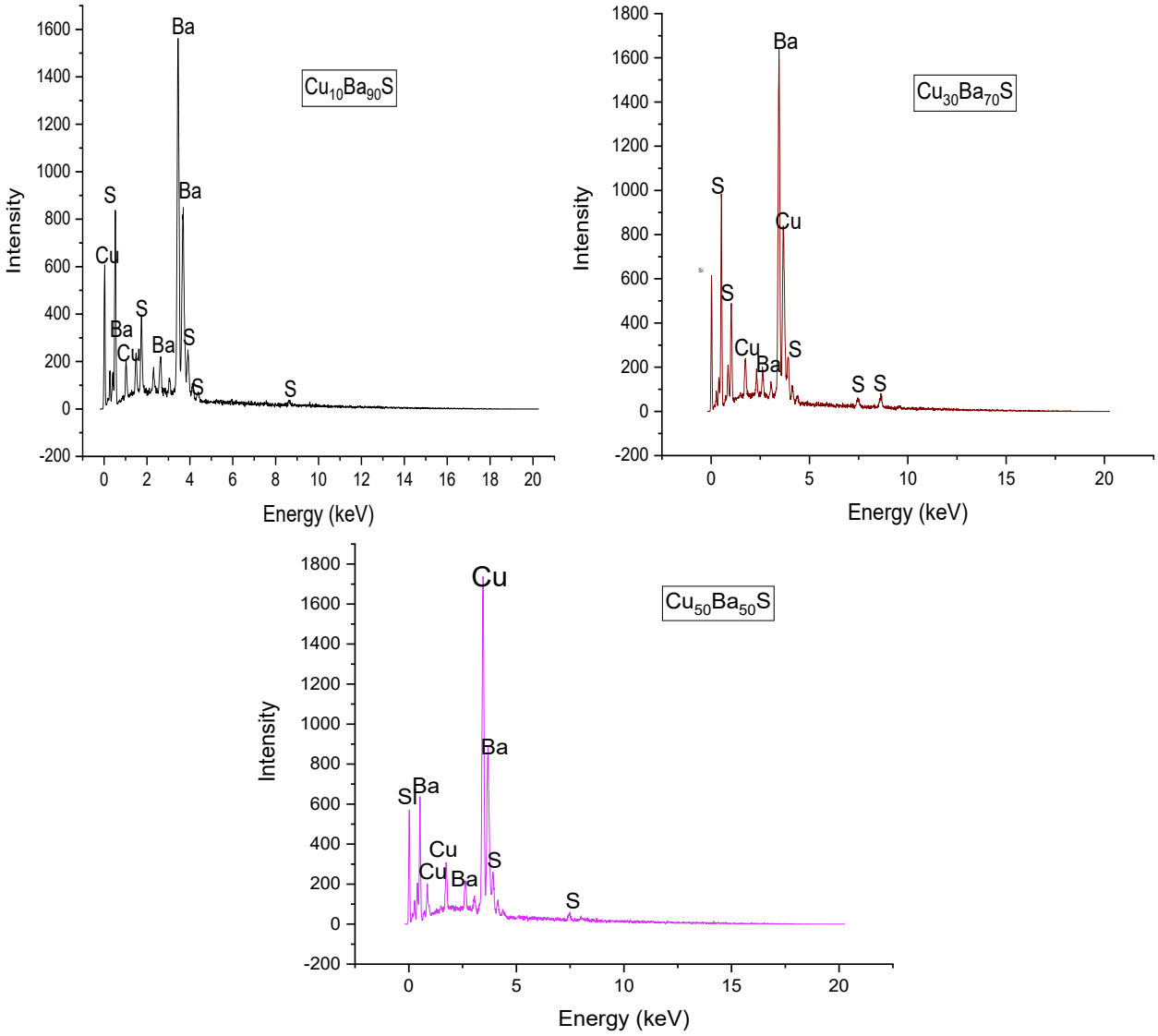

Figure 4. EDS Analysis of $Cu_xBa_{1-x}S$ TFs

Figure 4 shows the elemental compositions of the $Cu_xBa_{1-x}S$ TFs, confirming that the main elements within the films are copper (Cu), barium (Ba), and sulphur (S), with little or no detectable impurities. Compositional analysis, detailed in Table 3, indicates that the [Cu + Ba/S] ratio is not constant; rather, it increases as the copper concentration increases, suggesting that $Cu_xBa_{1-x}S$ films are non-stoichiometric [5]. Interestingly, increasing the doping concentration appears to accelerate nucleation in the starting solution's atoms, which consequently affects the elements present in $Cu_xBa_{1-x}S$ TFs, as evidenced by the diverse morphologies observed in SEM analyses. This behavior aligns with the findings of Ref. [5] regarding copper zinc iron sulphide TFs deposited via the CBD method. Additionally, Table 3 shows that the intensity (percentage) of copper diminishes with increasing copper concentration in $Cu_xBa_{1-x}S$ TFs. This phenomenon can be attributed to several factors, including the formation of secondary phases and changes in the local stoichiometry within the material [32]. For instance, in Cu-doped β-In2S3, the addition of copper can cause cuprous sulphide to precipitate, substantially affecting the elemental composition and thermoelectric characteristics [33]. Additionally, the smaller ionic radius of copper ions (relative to larger ions like barium) and the difficulty in achieving uniform mixing of precursors during solid-state reactions can lead to non-uniform dopant distribution [34, 35]. This non-uniformity can result in localized variations in elemental percentages and distorted surface morphologies [34]. Such non-uniformity may then cause the lattice constant and the elemental fraction of the doping element to gradually decline in accordance with Vegard's law [35]. This implies that a higher copper content significantly influences the physical properties of $Cu_xBa_{1-x}S$ thin films. To determine their optical properties, the transmittance (T) and absorbance (A) spectra of the deposited $Cu_xBa_{1-x}S$ thin films were recorded using a UV-1800 Spectrophotometer.

However, the reflectance (R) was subsequently assessed using Eq. (4) [16, 36]:

$$R + T + A = 1 \quad (4)$$

where R is the reflectance, T is the transmittance, and A is the absorbance given by [36]:

$$T = 10^{-A} \quad (5)$$

and

$$R = 1 - (T + A) \quad (6)$$

Figure 5(a) displays the optical transmittance spectra as a function of wavelength, revealing that the films possess high transmittance within the visible and near-infrared ranges. Sample $Cu_{10}Ba_{90}S$ had the highest transmittance at wavelength of above 500 m region. Also, sample $Cu_{50}Ba_{50}$ was found to be between $Cu_{10}Ba_{90}S$ and $Cu_{30}Ba_{70}S$ with increasing wavelength, likely due to the non-homogeneous nature of $Cu_xBa_{1-x}S$ TFs as observed by the SEM micrograph (Figure 3) [21]. This increase in transmittance with wavelength may be attributed to the formation of copper doped barium sulphide nano-particles [37] Therefore, the rise in copper concentrations makes the films more transparent. Moreover, the high transmittance seen in this study occurred because the films had increased crystallinity, which lowered grain boundary defects [26]. Films with such high transmittance could be useful as transparent conducting materials in LEDs and solar cells [37]. Similar observations have been reported in literature for semiconducting thin films [38, 39]. Figure 5(b) illustrates the optical absorbance of the films, indicating low absorbance in the ultraviolet region. This absorbance decreases with increasing wavelength up to the near-infrared region as doping concentrations increase. Generally, the films exhibit poor absorbance throughout the wavelength ranges.

However, the low absorbance observed in this study could be a result of a decrease in the number of defects as well as an elevation in grain sizes [40]. The reflectance spectra of the deposited thin films with different copper ion concentrations are illustrated in Figure 5(c). The reflectance values of all the films were found to be between 0 and 20. The plot reveals that doping with copper alters the reflectivity throughout the wavelength regions. Nevertheless, the reflectance values indicate that the deposited materials do not reflect light well, which makes them appropriate as a p-type material for solar cell applications [41]. In general, the reflectance of thin films tends to increase sharply at wavelengths shorter than 600 nm, which may be attributed to higher concentrations of copper. This observation is linked to the increase in copper doping, leading to greater surface roughness, as demonstrated in the SEM images. Furthermore, the low reflectance of these films makes them potentially useful as anti-reflection coatings [37, 42]. The energy gap (E_g) of the $Cu_xBa_{1-x}S$ TFs was estimated using the Tauc's formula [43, 44]:

$$\alpha h\nu = B(h\nu - E_g)^n \quad (7)$$

Here, the index 'n' can be 2, 3, 3/2 and 1/2, varying with the electronic transition responsible for absorption [43, 45]. Specifically, 'n' is 1/2 for direct allowed transitions, 2 for indirect allowed transitions, 3 for indirect forbidden transitions, and 3/2 for direct forbidden transitions [45]. E_g represents the energy gap, hν is the photon energy, and B is a constant related to the transition probability [45]. Figure 6(a) depicts a curve of the square of absorption $(\alpha h\nu)^2$ against photon energy (hν), and the energy gap of the deposited thin films is calculated [5]. This calculation involves extrapolating the linear region of the plot to where the square of absorption equals zero [45]. This single linear part indicates that direct transitions are dominant in the films. The estimated energy gap increased from 1.65 to 3.12 eV with copper doping (Figure 6a). The observed near-linear relationship between the energy gap and copper concentration arises from the difference in energy gaps between CuS and BaS thin films, with CuS exhibiting a larger gap [46, 47]. This upward shift in energy is consistent with established patterns for semiconducting thin films reported in the literature [6]. The increase in the direct optical band gap suggests an increase in crystalline size and a reduction in structural defects, as indicated by the XRD study [5]. This could also be a result of the Burstein-Moss effect [5]. When copper atoms are deeply doped into barium-sulphide films, the lower energy levels in the conduction bands are occupied by electrons, resulting in an increased Fermi level and wider optical band gaps [44]. Another possibility for the rise in the E_g can be attributed to the presence of secondary phases in small quantities that may not be detected within the films [37]. The increased copper incorporation modifies the energy gap, improving the films' suitability for electronic applications by enabling more short-wavelength photons to reach the absorber layer and generate a greater photocurrent than barium-sulphide thin films [5, 6].

The refractive index (n) of a material is a crucial property for many optical devices because it is strongly related to the material's electronic polarization [37, 48, 49]. The refractive index is connected to the electronic polarization of ions, as described by the following Eq. (8) [48].

$$n = \left(\frac{1+R}{1-R}\right) + \sqrt{\left(\frac{4R}{(1-R)^2}\right) - k^2} \quad (8)$$

Here, R is the reflectance, while k is the extinction coefficient of $Cu_xBa_{1-x}S$ thin films.

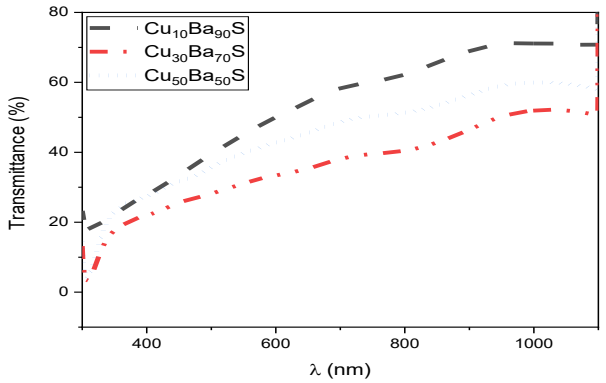

Figure 5(a). Transmittance spectra of $Cu_xBa_{1-x}S$ TFs

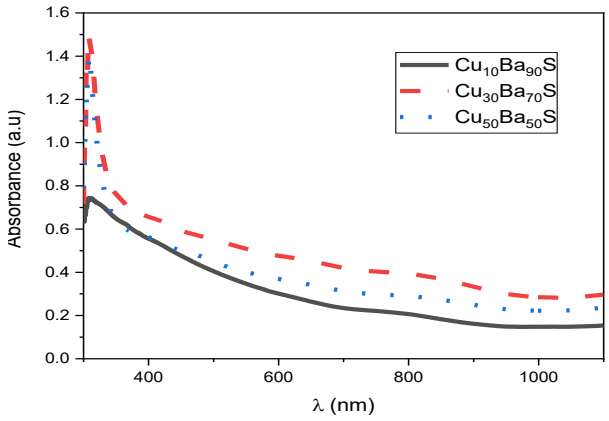

Figure 5(b). Absorbance spectra of $Cu_xBa_{1-x}S$ TFs

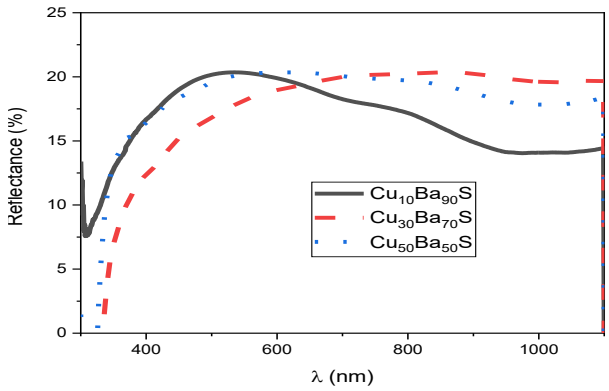

Figure 5(c). Reflectance spectra of $Cu_xBa_{1-x}S$ TFs

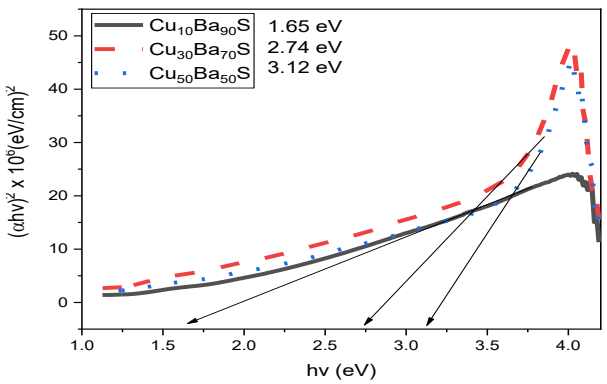

Figure 6(a). Square of absorption coefficient against photon energy of $Cu_xBa_{1-x}S$ TFs

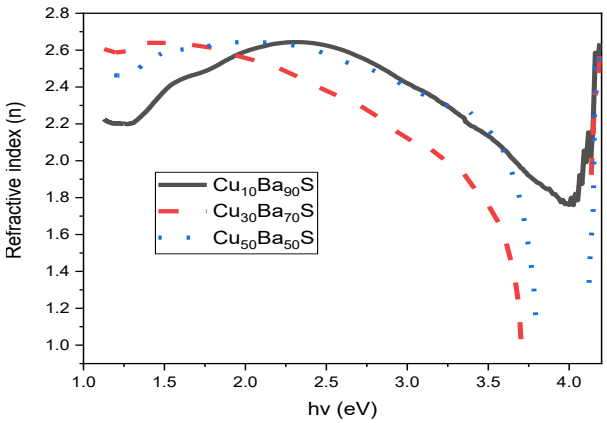

Figure 6(b). The refractive Index against photon energy of $Cu_xBa_{1-x}S$ TFs

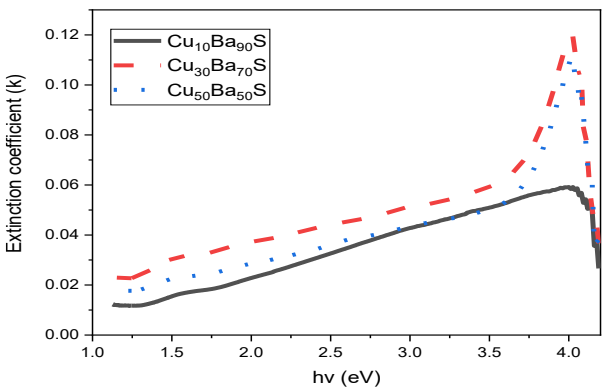

Figure 6(c). Extinction coefficient against photon energy of $Cu_xBa_{1-x}S$ TFs

Figure 6(b) shows a graph of n against photon energy. The graph indicates that the average n decreased as the photon energy of the $Cu_xBa_{1-x}S$ TFs increased. Furthermore, with increasing doping concentration, the refractive indexes varied from 2.30 to 2.54 at 2.5 eV. The observed variations in n-values might stem from the confinement of photon energy within the grain boundary structures of the films [16, 37]. The enhanced n-values of $Cu_xBa_{1-x}S$ TFs may be advantageous for improving the visual performance of optoelectronic applications such as quantum dot light-emitting diodes and liquid crystal displays, which depend on electronic display mechanisms [5]. The extinction coefficient k was determined utilizing the relationships outlined in the Eq. (9) [45, 49]:

$$k = \frac{\alpha\lambda}{4\pi} \quad (9)$$

where, λ denotes the wavelength of the spectrum. Figure 6(c) depicts the curve of k against photon energy, which reveals that k increases with both photon energy and doping concentration for all films. In general, the behavior of the extinction coefficient is caused by consecutive internal reflections or stored photon energy in grain boundaries [37].

Ref. [45] reported similar results for ternary thin films. Furthermore, the optical conductivity as an important parameter characterizes the relationship between the strength of the induced electric field and the induced current density across various frequencies [49]. The optical conductivity of $Cu_xBa_{1-x}S$ TFs was evaluated using the Eq. (10) [49, 50]:

$$\sigma_{opt} = \frac{\alpha nc}{4\pi} \quad (10)$$

In the formula, c denotes the speed of light. Figure 7(a) presents the optical conductivity of the films as a function of photon energy across various doping concentrations. It was generally observed that an increase in copper concentration leads to a higher charge carrier density in the films, consequently enhancing the σ_{opt} of the deposited materials [48]. The high value of the σ_{opt} observed at photon energies above 2.5 eV is due to the expansion of the energy gap between the valence and conduction bands with increasing doping concentration [37, 48, 49]. Therefore, more photon energy is needed for electrons to move from the valence band to the conduction band. This behavior is consistent with previously reported results [10].

On the other hand, Eqs. (11) and (12) were used to determine the real and imaginary components of the dielectric constant [10, 45, 51]:

$$\varepsilon_r = n^2 - k^2 \quad (11)$$

and

$$\varepsilon_i = 2nk \quad (12)$$

These equations use ε_r and ε_i to represent the real and imaginary parts of the dielectric constants. Figures 7(b) and 7(c) show how ε_r and ε_i vary with photon energy. Similar to the refractive index, the real dielectric constant varies with both photon energy and copper concentration. Nonetheless, the plot indicates that increasing copper concentrations, decreases the magnitude of ε_r along the photon energy range. This pattern within the films is comparable to those reported in Ref. [10], linking the development to the correlations between the extinction coefficient, refractive index, and real dielectric constant, as stated in Eq. (11). Meanwhile, Figure 7(c) shows the relationship between photon energy and the imaginary dielectric constant (ε_i). The graph reveals a significant increase in the films, influenced by both the photon energy range and the amount of copper deposited. Unlike the real dielectric constant, the plot shows that the films increase with low values of the imaginary dielectric constant. Overall, the variations observed in the imaginary dielectric constant can likely be ascribed to the energy absorption characteristics of the deposited TFs within a charged area [6].

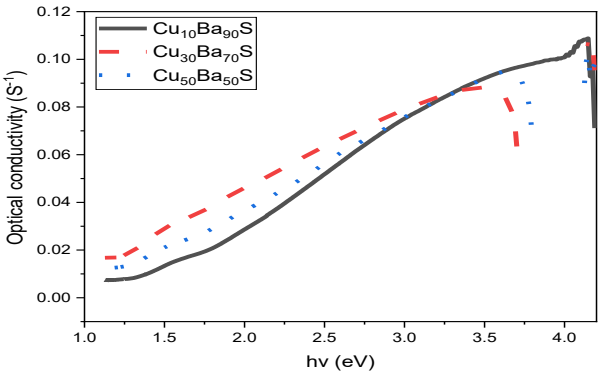

Figure 7(a). Optical conductivity against photon energy of $Cu_xBa_{1-x}S$ TFs

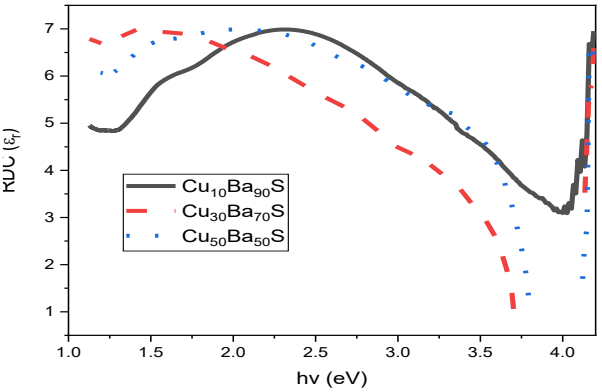

Figure 7(b). Real dielectric constant against photon energy of $Cu_xBa_{1-x}S$ TFs

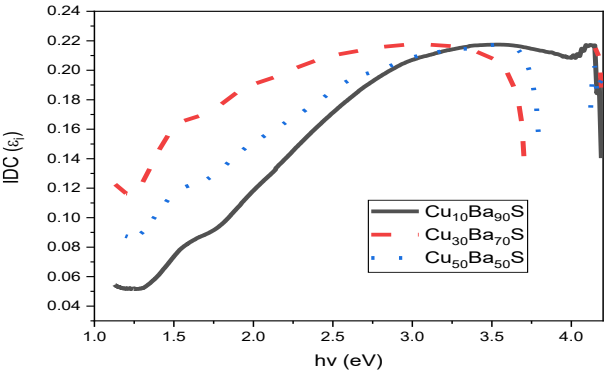

Figure 7(c). Imaginary dielectric constant against photon energy of $Cu_xBa_{1-x}S$ TFs

4. Conclusion

$Cu_xBa_{1-x}S$ thin films were successfully synthesized utilizing the CBD method. The approach provides a novel method for producing $Cu_xBa_{1-x}S$ thin films using chemical precursors. It has been concluded that the doping concentration has a direct influence on the properties of the deposited films. The EDX measurements confirmed that the films are composed of copper, barium, and sulphur in varied elemental compositions. SEM indicated an aggregation of grains of various morphological forms and sizes that increased with copper concentration.

10.57647/jtap.2026.2002.12

The films exhibited high transmittance in the UV region, with the energy gap increasing alongside the doping concentration.

The exhibited properties of the films at varying concentrations confirm their potential as a suitable material for different optoelectronic devices. The following areas require further research: utilizing hall effect measurements is crucial for determining the mobility, Hall coefficients, and carrier concentrations in the TFs. Beyond this, X-ray photoelectron spectroscopy (XPS) analysis can provide insights into the elemental composition, chemical state, electronic structure, as well as the density of electronic states of the material.

Furthermore, conducting photoluminescence and electroluminescence measurements would be invaluable in revealing the films' luminescent characteristics for industrial applications.

Authors Contribution
The authors contributed equally to the preparation and writing of the manuscript.

Availability of data and materials
The datasets used and analyzed in the current research are available through the corresponding author upon legitimate requests.

Conflict of interests
The datasets used and analyzed in the current research are available through the corresponding author upon legitimate requests.

References

[1] M. M. Hasan, S. Hossain, M. Mofijur, Z. Kabir, I. A. Badruddin, T. M. Yunus Khan, and E. Jassim, "Harnessing Solar Power: A Review of Photovoltaic Innovations, Solar Thermal Systems, and the Dawn of Energy Storage Solutions," Energies, vol. 16, no. 18, art. 6456, Sep. 2023, doi: https://doi.org/10.3390/en16186456. MDPI

[2] N. Kannan and D. Vakeesan, "Solar Energy for Future World—A Review," Renew. Sustain. Energy Rev., vol. 62, pp. 1092–1105, 2016, doi: https://doi.org/10.1016/j.rser.2016.05.022

[3] E. J. Onyeka, "Design and Analysis of 1.0 KVA Grid-Connected Micro-Grid PV-Systems for a Residential Setting in Delta State, Nigeria," Dutse J. Pure Appl. Sci. (DUJOPAS), vol. 10, no. 1a, pp. 118–128, Mar. 2024, doi: https://doi.org/10.4314/dujopas.v10i1a.13

[4] A. Shahsavari and M. Akbari, "Potential of Solar Energy in Developing Countries for Reducing Energy-Related Emissions," Renew. Sustain. Energy Rev., vol. 90, pp. 275–291, Jun. 2018, doi: https://doi.org/10.1016/j.rser.2018.03.021

[5] J. O. Emegha, K. E. Ukhurebor, U. O. Aigbe, J. Damisa, A. V. Babalola, and S. Olofinjana, "Synthesis and Characterization of Copper Zinc Iron Sulphide (CZFS) Thin Films," Heliyon, vol. 8, no. 8, p. e10331, Aug. 2022, doi: https://doi.org/10.1016/j.heliyon.2022.e10331

[6] J. O. Emegha et al., "Synthesis and Characterization of Zinc Cobalt Sulphide Nanofilms for Optoelectronic Applications," CINORG., vol. 4, p. 100068, 2024, doi: https://doi.org/10.1016/j.cinorg.2024.100068

[7] M. A. Green et al., "Solar Cell Efficiency Tables (Version 47)," Prog. Photovolt. Res. Appl., vol. 24, no. 1, pp. 3–11, 2016, doi: https://doi.org/10.1002/pip.2828

[8] M. Scarpulla, B. McCandless, A. Phillips, et al., "CdTe-Based Thin Film Photovoltaics: Recent Advances, Current Challenges and Future Prospects," Sol. Energy Mater. Sol. Cells, vol. 255, p. 112289, 2023, doi: https://doi.org/10.1016/j.solmat.2023.112289

[9] A. Hussain, R. Ahmed, et al., "Synthesis and Characterization of Thermally Evaporated Copper Bismuth Sulphide Thin Films," Surf. Coat. Technol., vol. 320, pp. 404–408, 2017, doi: https://doi.org/10.1016/j.surfcoat.2016.12.012

[10] F. O. Efe, B. Olofinjana, O. Fasakin, M. A. Eleruja, and E. O. B. Ajayi, "Compositional, Structural, Morphological, Optical and Electrical Property Evolutions in MOCVD Cu-Zn-S Thin Films Prepared at Different Temperatures Using a Single Solid Source Precursor," J. Electron. Mater., vol. 48, no. 10, pp. 1007–1017, 2019, doi: https://doi.org/10.1007/s11664-019-07636-2

[11] K. K. Subedi et al., "Semi-Transparent p-Type Barium Copper Sulfide as a Back Contact Interface Layer for Cadmium Telluride Solar Cells," Sol. Energy Mater. Sol. Cells, vol. 218, p. 110764, 2020, doi: https://doi.org/10.1016/j.solmat.2020.110764

[12] Y. Han, S. Siol, Q. Zhang, and A. Zakutayev, "Optoelectronic Properties of Strontium and Barium Copper Sulfides Prepared by Combinatorial Sputtering," Chem. Mater., vol. 29, pp. 8239–8248, 2017, doi: https://doi.org/10.1021/acs.chemmater.7b02945

[13] A. Márquez, J. Sun, H. Stange, H. Ali, et al., "High-Temperature Decomposition of Cu_2BaSnS_4 with Sn Loss Reveals Newly Identified Compound $Cu_2Ba_3Sn_2S_8$," J. Mater. Chem. A, vol. 8, pp. 11346–11353, 2020, doi: https://doi.org/10.1039/D0TA02348E

[14] Y. Wang, M. Liu, F. Huang, L. Chen, H. Li, X. Lin, W. Wang, and Y. Xia, "Solution-Processed p-Type Transparent Conducting $BaCu_2S_2$ Thin Film," Chem. Mater., vol. 19, pp. 3102–3104, 2007,

doi: https://doi.org/10.1021/cm070541v

[15] A. A. Taha, M. H. S. Al-Jawad, and M. Abdulah, "Preparation and Characterization of Nanostructure CuS for Biological Activity," Mod. Phys. Lett. B, vol. 33, no. 30, p. 1950374, 2019, doi: https://doi.org/10.1142/S0217984919503743

[16] S. M. H. Al-Jawad et al., "Influence of Nickel Doping Concentration on the Characteristics of Nanostructure CuS Prepared by Hydrothermal Method for Antibacterial Activity," Surf. Rev. Lett., vol. 28, no. 1, p. 2050031, 2021, doi: https://doi.org/10.1142/S0218625X20500316

[17] O. N. Hussein, S. M. H. Al-Jawad, and N. J. Imran, "Efficient Antibacterial Activity Enhancement in Fe/Mn Co-Doped CuS Nanoflowers and Nanosponges," Bull. Mater. Sci., vol. 46, p. 139, 2023, doi: https://doi.org/10.1007/s12034-023-02964-w

[18] S. Gupta et al., "Temperature-Dependent Study of the Fabricated ZnS/p-Si Heterojunction," Physica B-Condensed Matter, vol. 657, p. 414831, 2023, doi: https://doi.org/10.1016/j.physb.2023.414831

[19] D. E. Elete, J. O. Emegha, N. O. Nenuwe, and O. W. Omagbemi, "Synthesis and Characterization of Chemical Bath Deposited Copper Doped Lead Sulfide Thin Films," Bull. Chem. Soc. Ethiop., vol. 37, no. 5, pp. 1237–1251, 2023, doi: https://doi.org/10.4314/bcse.v37i5.14

[20] A. Kumar et al., "Fabrication of Enhanced Performance Visible-Light Photodetector Based on Ag/ZnS/p-Si/Ag Heterojunction Grown by Chemical Bath Deposition," Mater. Today Commun., vol. 38, p. 108252, 2024, doi: https://doi.org/10.1016/j.mtcomm.2024.108252

[21] J. O. Emegha, A. El-Rayyes, Y. S. Itas, and M. U. Khandaker, "The Impact of Iron Concentration on the Structural and Optical Properties of Iron Lead Sulphide Thin Films," J. Indian Chem. Soc., vol. 102, no. 10, p. 102085, 2025, doi: https://doi.org/10.1016/j.jics.2025.102085

[22] J. Damisa and J. O. Emegha, "Growth and Optical Analysis of Cobalt Tin Sulphide Thin Films Using SILAR Technique," RJEES, vol. 6, pp. 642–648, 2021, doi: https://doi.org/10.5281/zenodo.5805219

[23] P. More et al., "Annealing Effect on Cu_2S Thin Films Prepared by Chemical Bath Deposition," AIP Conf. Proc., vol. 1728, no. 1, p. 020489, 2016, doi: https://doi.org/10.1063/1.4946513

[24] K. K. Subedi et al., "Semi-transparent p-type barium copper sulfide as a back contact interface layer for cadmium telluride solar cells," Sol. Energy Mater. Sol. Cells, vol. 218, p. 110764, 2020, doi: https://doi.org/10.1016/j.solmat.2020.110764

[25] N. A. Karim, N. A. Ludin, M. A. Mat-Teridi, S. Sepeai, M. A. Ibrahim, M. Kouhnavard, K. Sopian, and H. Arakawa, "Effects of deposition time on cobalt sulphide thin films electrode formation," Malaysian J. Anal. Sci., vol. 22, no. 1, pp. 80–86, 2018,

[26] J. O. Emegha, K. E. Ukhurebor, U. O. Aigbe, B. Olofinjana, S. O. Azi, and M. A. Eleruja, "Effect of deposition temperature on the properties of copper–zinc sulphide thin films using mixed copper and zinc dithiocarbamate precursors," GU J. Sci., vol. 35, no. 4, pp. 1556–1570, 2022,

[27] J. Damisa, J. O. Emegha, and I. L. Ikhioya, "Deposition Time Induced Structural and Optical Properties of Lead Tin Sulphide Thin Films," J. Nig. Soc. Phys. Sci., vol. 3, no. 4, pp. 455–458, 2021, doi: https://doi.org/10.46481/jnsps.2021.157

[28] A. A. Akl and A. S. Hassanien, "Microstructure characterization of Al–Mg alloys by X-ray diffraction line profile analysis," Int. J. Adv. Res., vol. 2, no. 11, pp. 1–9, 2014,

[29] A. A. Akl and A. S. Hassanien, "Comparative microstructural studies using different methods: Effect of Cd-addition on crystallography, microstructural properties, and crystal imperfections of annealed nano-structural thin CdxZn1−xSe films," Physica B, vol. 620, p. 413267, 2021, doi: https://doi.org/10.1016/j.physb.2021.413267

[30] Y. B. Xin and C. J. Summers, "Grain growth in thin-film strontium sulfide electroluminescent phosphors," Appl. Phys. Lett., vol. 75, no. 13, pp. 1860–1862, 1999, doi: https://doi.org/10.1063/1.124852

[31] A. C. Adebisi, M. S. Eluyemi, J. O. Emegha, et al., "Thermistor behavior of non-stoichiometric cadmium sulfide thin films," J. Mater. Sci.: Mater. Electron., vol. 36, p. 1309, 2025, doi: https://doi.org/10.1007/s10854-025-15435-1

[32] J. A. Márquez et al., "High-temperature decomposition of Cu_2BaSnS_4 with Sn loss reveals newly identified compound $Cu_2Ba_3Sn_2S_8$," J. Mater. Chem. A, vol. 8, pp. 11346–11353, 2020, doi: https://doi.org/10.1039/D0TA02348E

[33] Y. Chen, F. Li, W. Wang, Z. Zheng, J. Luo, P. Fan, and T. Takeuchi, "Optimization of thermoelectric properties achieved in Cu-doped β-In_2S_3 bulks," J. Alloys Compd., vol. 782, pp. 641–647, 2019,

doi: https://doi.org/10.1016/j.jallcom.2018.12.138

[34] S. Puthran, G. S. Hegde, A. N. Prabhu, et al., "A comprehensive experimental and DFT analysis on thermoelectric properties of Sb, Te co-doped Bi_2Se_3 polycrystals," J. Mater. Sci., vol. 59, pp. 11817–11834, 2024, doi: https://doi.org/10.1007/s10853-024-09865-1

[35] B. Tandon, S. Ghosh, and D. J. Milliron, "Dopant Selection Strategy for High-Quality Factor Localized Surface Plasmon Resonance from Doped Metal Oxide Nanocrystals," Chem. Mater., vol. 31, no. 18, pp. 7752–7760, 2019, doi: https://doi.org/10.1021/acs.chemmater.9b02917

[36] J. O. Emegha, T. O. Fowodu, T. Ede, and E. C. Odunze, "Preparation and Optical Characterization of Barium Sulphide Thin Films," SLUJST, vol. 10, no. 2, pp. 258–267, 2025, doi: https://doi.org/10.56471/slujst.v10i2.127

[37] J. O. Emegha, M. C. Okafor, and K. E. Ukhurebor, "Optical properties of copper-zinc sulphide network from mixed single solid source precursors of copper and zinc dithiocarbamates," Walailak J. Sci. & Tech., vol. 18, no. 9, pp. 1–11, 2021, doi: https://doi.org/10.48048/WJST.2021.9535

[38] I. L. Ikhioya, E. O. Onah, M. Maaza, and F. I. Ezema, "Influence of precursor pH on the optical and electrical properties of electrochemically deposited cobalt-doped ZnSe thin films for photovoltaic application," Curr. Res. Green Sustain. Chem., vol. 5, p. 100286, 2022, doi: https://doi.org/10.1016/j.crgsc.2022.100286

[39] A. Habeebullah, A. B. Alabi, A. O. Babalola, E. D. Kajewole, T. J. Adeleke, and T. Akomolafe, "Synthesis and Characterization of a Dual-Doped Zinc Oxide [(Na, N):ZnO] Nanoparticles by Wet Chemical Method," Afr. Rev. Phys., vol. 13, 2018,

[40] E. O. Ojegu, R. A. Daniel-Umeri, E. C. Nwaokorongwu, N. Alghamdi, and I. L. Ikhioya, "Optimization of silver ion concentration into the lattice of zinc oxide nanoparticles synthesized via a hydrothermal approach," Nigerian J. Technol. Dev., vol. 21, no. 4, pp. 145–158, 2024,

[41] O. E. Osoro, Characterization of CuxOy-ZnO:Sn P-N Junction for Solar Cell Applications, M.Sc Thesis, Dept. of Physics, Kenyatta Univ., 2011.

[42] A. V. Babalola, V. Oluwasusi, V. A. Owoeye, J. O. Emegha, D. A. Pelemo, A. Y. Fasasi, U. M. Gurku, S. O. Alayande, S. Yusuf, and B. Saje, "Effect of tin concentrations on the elemental and optical properties of zinc oxide thin films," Heliyon, vol. 10, p. e23190, 2024, doi: https://doi.org/10.1016/j.heliyon.2023.e23190

[43] J. Damisa and J. O. Emegha, "XRD and UV-Vis Spectroscopic Studies of Lead Tin Sulphide (PbSnS) Thin Films," Trends Sci., vol. 18, no. 20, p. 16, 2021, doi: https://doi.org/10.48048/tis.2021.16

[44] T. O. Fowodu et al., "Influence of varying iron ion concentration and SILAR cycle on the optical properties of iron copper sulphide (FeCuS) thin films on different substrates," NIJEST, vol. 9, no. 1, pp. 278–289, 2025, doi: https://doi.org/10.36263/nijest.2025.01.36

[45] J. Damisa, B. Olofinjana, O. Ebomwonyi, F. Bakare, and S. O. Azi, "Morphological and optical study of thin films of $CuAlS_2$ deposited by metal organic chemical vapour deposition technique," Mater. Res. Express, vol. 4, pp. 1–10, 2017, doi: https://doi.org/10.1088/2053-1591/aa5abf

[46] K. A. Mohammed, S. M. Ahmed, and R. Y. Mohammed, "Investigation of Structure, Optical, and Electrical Properties of CuS Thin Films by CBD Technique," Crystals, vol. 10, p. 684, 2020, doi: https://doi.org/10.3390/cryst10080684

[47] D. N. Okoli, "Optical Properties of Barium Sulphide Thin Films Prepared by Chemical Bath Deposition Technique," IOSR-JAP, vol. 7, no. 4, pp. 10–15, 2015,

[48] A. M. Alsaad, Q. M. Al-Bataineh, A. A. Ahmad, Z. Albataineh, and A. Telfah, "Optical band gap and refractive index dispersion parameters of boron-doped ZnO thin films: A novel derived mathematical model from the experimental transmission spectra," Optik, vol. 211, p. 164641, 2020, doi: https://doi.org/10.1016/j.ijleo.2020.164641

[49] H. Y. S. Al-Zahrani, I. M. El Radaf, and A. A. Lahmar, "Study on the Impact of Vanadium Doping on the Structural, Optical, and Optoelectrical Properties of ZnS Thin Films for Optoelectronic Applications," Micromachines, vol. 16, p. 337, 2025, doi: https://doi.org/10.3390/mi16030337

[50] A. S. Hassanien and A. A. Akl, "Influence of Composition on Optical and Dispersion Parameters of Thermally Evaporated Non-Crystalline $Cd_{50}S_{50-x}Se_x$," J. Alloys Compd., vol. 648, pp. 280–290, 2015, doi: https://doi.org/10.1016/j.jallcom.2015.06.006

[51] B. Olofinjana et al., "Single solid source precursor route to the synthesis of MOCVD Cu–Cd–S thin films," Mater. Res. Express, vol. 6, pp. 1–17, 2019, doi: https://doi.org/10.1088/2053-1591/ab07e3